

JGR Solid Earth

RESEARCH ARTICLE

10.1029/2020JB021362

Key Points:

- A clustering analysis is performed to investigate the spatiotemporal correlation between seismicity and injection activity in western Canada
- Seismotectonic state of the injection sites is quantitatively characterized using the estimates of the seismogenic index
- Statistical models are presented to forecast the magnitudes of the largest expected events induced by deep fluid injection

Supporting Information:

Supporting Information may be found in the online version of this article.

Correspondence to:

R. M. H. Dokht,
ramin.mohammadhosseinidokht@
canada.ca

Citation:

Dokht, R. M. H., Kao, H., Babaie Mahani, A., & Visser, R. (2021). Spatiotemporal analysis of seismotectonic state of injection-induced seismicity clusters in the Western Canada Sedimentary Basin. *Journal of Geophysical Research: Solid Earth*, 126, e2020JB021362. <https://doi.org/10.1029/2020JB021362>

Received 16 NOV 2020
Accepted 8 MAR 2021

© 2021. Her Majesty the Queen in Right of Canada. Reproduced with the permission of the Minister of Natural Resources Canada.

Spatiotemporal Analysis of Seismotectonic State of Injection-Induced Seismicity Clusters in the Western Canada Sedimentary Basin

Ramin M. H. Dokht¹ , Honn Kao^{1,2} , Alireza Babaie Mahani³, and Ryan Visser^{1,3}

¹Pacific Geoscience Centre, Geological Survey of Canada, Natural Resources Canada, Sidney, BC, Canada, ²School of Earth and Ocean Sciences, University of Victoria, Victoria, BC, Canada, ³Geoscience BC, Vancouver, BC, Canada

Abstract The observations of spatiotemporal distribution of seismicity in western Canada indicate that the occurrence of earthquakes is tied to the hydraulic fracturing operations and disposal of coproduced wastewater. In this study, we investigate the temporal changes in the frequency-magnitude distributions for multiple clusters of induced events in regions where the level of background seismicity is low. The induced events are clustered into six major groups using density-based spatial and soft clustering algorithms based on their epicenters. Each cluster is identified by different distributions of earthquake magnitudes and injection scenarios. The linear relationship between the number of induced earthquakes and cumulative injection volume enables us, on a regional scale, to quantitatively characterize the seismotectonic conditions of the clusters using the estimates of the seismogenic indices. The seismogenic index provides a means to estimate the occurrence probability of earthquakes with a given magnitude induced during injection. The calculated seismogenic indices agree very well with the expected seismic response to hydraulic fracturing and wastewater disposal and show a strong correlation with tectonically accumulated strain energy. Statistical models based on the seismogenic index can be employed to mitigate the potential risk of large magnitude induced events.

1. Introduction

The Western Canada Sedimentary Basin (WCSB), a tectonically quiescent zone, has experienced a substantial increase in the rate of seismicity; from an average of one earthquake with magnitude (local magnitude M_L or moment magnitude M_W) ≥ 1.5 per year prior to 2000 (reported in the Canadian National Earthquake Database) to an annual average of $>800 M_L \geq 1.5$ earthquakes in recent years (Visser et al., 2017, 2020). Most of the recent earthquakes within the WCSB have been limited to specific areas associated with stress perturbations caused by anthropogenic activities including mining operations (Dokht et al., 2020; Fereidoni & Atkinson, 2017; Stern et al., 2013) and fluid injection or withdrawal related to the development of unconventional hydrocarbons (Atkinson et al., 2016; Babaie Mahani et al., 2017; Bao & Eaton, 2016; Schultz et al., 2014). While an increased seismicity rate in the central and eastern United States has been linked to the disposal of large volumes of waste fluids (Ellsworth, 2013; Goebel et al., 2017; Keranen et al., 2014; Yeck et al., 2017), injection-induced earthquakes (IIE) in western Canada are found to be mostly associated with hydraulic fracturing (HF) within the thick sedimentary formations (Eaton & Schultz, 2018; Farahbod et al., 2015; Schultz et al., 2017), where the volume of waste fluid injection is found to be relatively low (Atkinson et al., 2016; Schultz et al., 2020).

The epicentral locations of IIEs in western Canada appear to follow a NW-SE trend that places constraints on their spatial distribution (Figure 1). A spatiotemporal correlation analysis between injection operations and seismicity in the WCSB indicates a per-well incidence rate of $<1\%$ for earthquakes of significant magnitudes (M_L or $M_W \geq 3$; Atkinson et al., 2016). The HF activity has induced the largest earthquakes in this region, including the 2014 $M_W 4.5$, 2015 $M_W 4.6$, and 2016 $M_W 3.9$ earthquakes in northern Montney Play, northeastern British Columbia (NE BC; Babaie Mahani et al., 2017; Kao, Visser, et al., 2018), the 2015 $M_W 3.9$ and 2016 $M_W 4.1$ events near Fox Creek, Alberta (AB; Clerc et al., 2016; Wang et al., 2017) and the 2018 $M_W 4.6$ Septimus earthquake in NE BC (Babaie Mahani et al., 2019), which triggered the immediate cessation of injection operations.

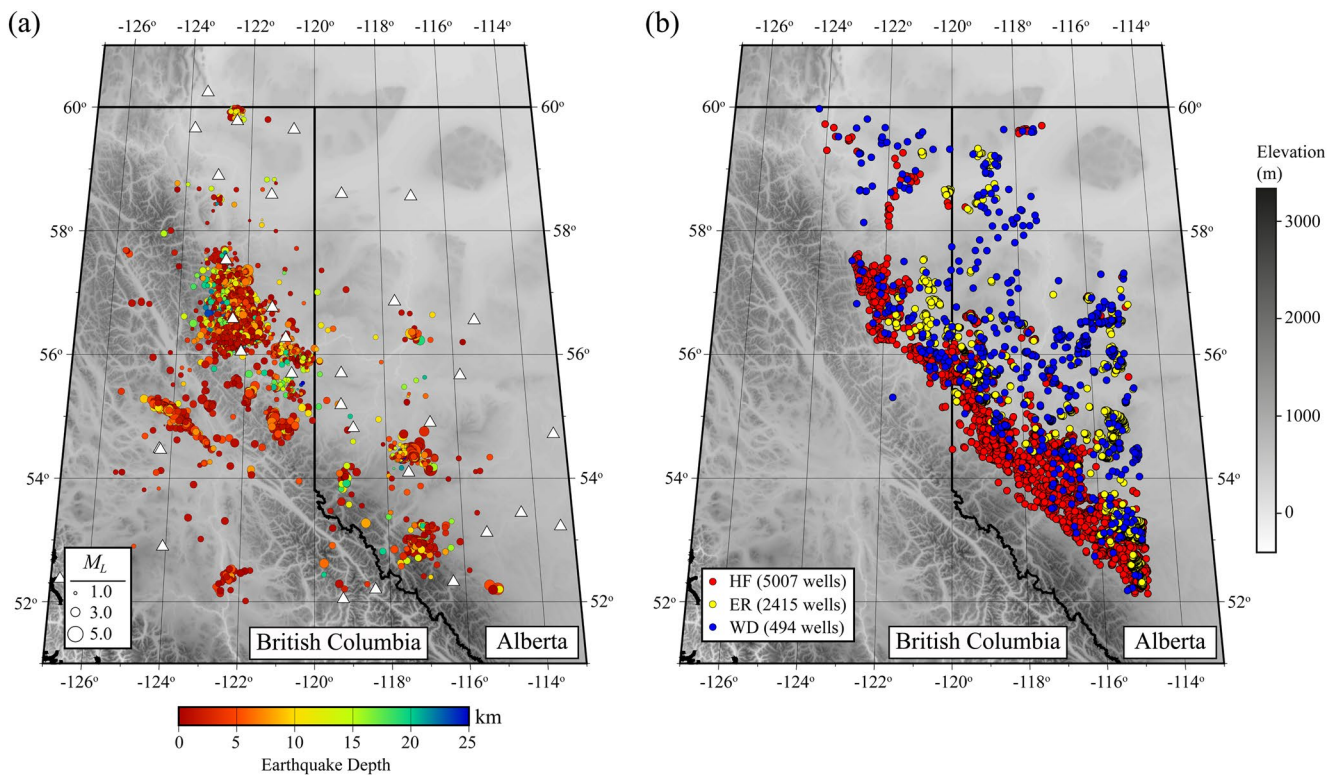


Figure 1. (a) Distributions of earthquake epicenters (circles) and locations of seismic stations (white triangles). The magnitudes and depths of earthquakes can be identified by their sizes and colors, respectively (Visser et al., 2017). (b) A map of the hydraulic fracturing (HF; red circles), enhanced recovery (ER; yellow circles), and wastewater disposal (WD; blue circles) well locations. The total number of each well type is reported in the legend. The earthquake and fluid injection data have been collected for the period of January 2014 to December 2016.

In Peace River, northern AB, pore pressure increase due to fluid diffusion, resulting from the disposal of waste fluid in the porous carbonate buildups of the Leduc Formation, and reactivation of deep-seated faults are considered to be the primary cause of the increased seismicity rate (Anderson & Eaton, 2016; Hubbard et al., 1999; Shell Recovery Process, 2009). Within the Duvernay Play of central AB, the distribution of HF-induced seismicity reveals a significant spatial correlation with the margins of the Devonian carbonate reefs (Schultz et al., 2016). Wang et al. (2017) proposed a system of subvertical basement-rooted faults, extending into the sedimentary cover, which can influence the structural development of the reef margins. Hydraulic communication between the shallow fractures and basement faults can potentially promote failure on optimally oriented faults and trigger large earthquakes within the crystalline basement (Bao & Eaton, 2016; Chopra et al., 2017; Galloway et al., 2018).

Recent studies of pressure communication between the injection point and the locations of induced events during the HF treatment within the Montney shale gas basin in NE BC suggest that elevated pore pressure and poroelastic stress transfer control the nucleation of seismicity in the immediate vicinity of injection wells and the reactivation of offset faults, respectively, at short time scales after injection (Peña Castro et al., 2020; Roth et al., 2020; Yu et al., 2019). In the Horn River Basin, located in northern BC, the occurrence of IIEs has been linked to HF fluid injection in a deep bituminous shale formation and disposal of coproduced wastewater into the overlying porous carbonate unit within an active fault zone (BC Oil & Gas Commission, 2012; Farahbod et al., 2015; Verdon & Budge, 2018).

Several different mechanisms and controlling factors have been proposed to explain the occurrence of induced seismicity in the WCSB. In addition to elevated pore pressure, the presence of a permeable conduit within the fracture zone and proximity to critically stressed faults (Bao & Eaton, 2016; Peña Castro et al., 2020; Van der Baan & Calixto, 2017), high formation-overpressure is found to be strongly correlated with increased likelihood of HF-induced seismicity in the Montney and Duvernay Plays (Eaton &

Schultz, 2018). A comparison between crustal deformation and the regional seismic pattern in the WCSB suggests that tectonic moment rate plays a major role in the occurrence of IIEs over an extended period of time (Kao, Hyndman, et al., 2018).

In this study, we systematically investigate the spatiotemporal distribution of seismicity in western Canada and its correlation with large-scale changes in fluid injection rate for a 3-year time period commenced in January 2014 (Figure 1). The growing concern over the occurrence of large IIEs in AB led to the implementation of a traffic light system as a regulatory response aimed at mitigating the associated seismic risk (Alberta Energy Regulator, 2015). Similarly, the occurrence of induced earthquakes with local magnitudes greater than 4 leads to suspension of operations in NE BC by regulations of the British Columbia Oil and Gas Commission (BCOGC; Babaie Mahani et al., 2019; Kao et al., 2016). Moreover, monitoring areas have been implemented in NE BC where operators must provide seismological details after the occurrence of ground accelerations in excess of 0.008 g. To assist the regulatory authorities and operators, we present statistical models of IIEs for multiple geographic clusters to estimate the occurrence probabilities of significant magnitude events in the WCSB. The models are based on the seismotectonic conditions of injection sites (Shapiro et al., 2010) and allow us to forecast the magnitude of the largest event that can be potentially induced during fluid injection. We take advantage of a detailed injection data set and a comprehensive earthquake catalog compiled for the WCSB to study the variation in the behavior of induced seismicity, controlled by fluid injection volume, in different areas.

2. Data Set and Method

2.1. Data Set

The seismicity analyzed in this study was recorded by 38 broadband and short-period permanent stations on three channels between January 2014 and December 2016 (Visser et al., 2017; see Figure 1a and Table S1 for detailed information on the recording stations). Over this time period, the Geological Survey of Canada of Natural Resources Canada has cataloged 4,863 seismic events in NE BC and western AB, which have been largely attributed to injection operations during the development of unconventional hydrocarbon resources (Atkinson et al., 2016; Kao, Visser, et al., 2018; Schultz et al., 2014). The reported events have M_L magnitudes ranging from 0.08 to 4.94 with an average depth of ~5 km (see Figure 1a; we refer readers to Visser et al. (2017) and Kao, Hyndman, et al. (2018) for details on earthquake source parameter calculation).

Next, to explore the relationship between changes in seismicity and injection rates, we consider a data set of injection parameters from hydraulic fracturing (HF), enhanced recovery (ER), and wastewater disposal (WD) wells in western Canada that have been active during the study period (see Figure 1b). The fluid injection parameters have been collected from BCOGC for BC and the geoSCOUT software has been used to extract the injection well data associated with AB (Kao, Hyndman, et al., 2018). The combined injection data set includes 5007, 2415, and 494 HF, ER, and WD wells, respectively, with the corresponding fractions of 13.4%, 61.7%, and 24.9% of the total injected fluid volume (Figures S1 and S2).

2.2. Earthquake Clustering: DBSCAN and Fuzzy C-Means

To investigate the spatiotemporal characteristics of IIEs, we cluster earthquakes based on their epicentral locations using the Density-Based Spatial Clustering of Applications with Noise (DBSCAN) algorithm (Ester et al., 1996). Unlike other clustering techniques, DBSCAN is a spatial clustering algorithm which can be utilized to discover an arbitrary number of clusters of arbitrary shapes (Borah & Bhattacharyya, 2004). DBSCAN defines clusters as connected areas of high earthquake density, above a given threshold. Any two earthquakes within a cluster are mutually density-connected if they are both density-reachable from a core point. Any earthquake satisfying the density threshold condition of containing a minimum number of events, $minPts$, in its neighborhood of radius ϵ , can be considered as a core point (Arlia & Coppola, 2001; Schubert et al., 2017). The initial earthquake clusters are obtained using a neighborhood radius of $\epsilon = 6$ km and a minimum number of neighboring events $minPts = 20$. The neighborhood radius of 6 km is determined as the sum of the average, 1.8 km, and two standard deviations, 4 km, of the major axis lengths of error ellipses of the entire earthquake catalog (Figure S3). This results in eight distinct earthquake clusters, five of which are spatially correlated, and can be potentially associated with injection activity (Figure 2).

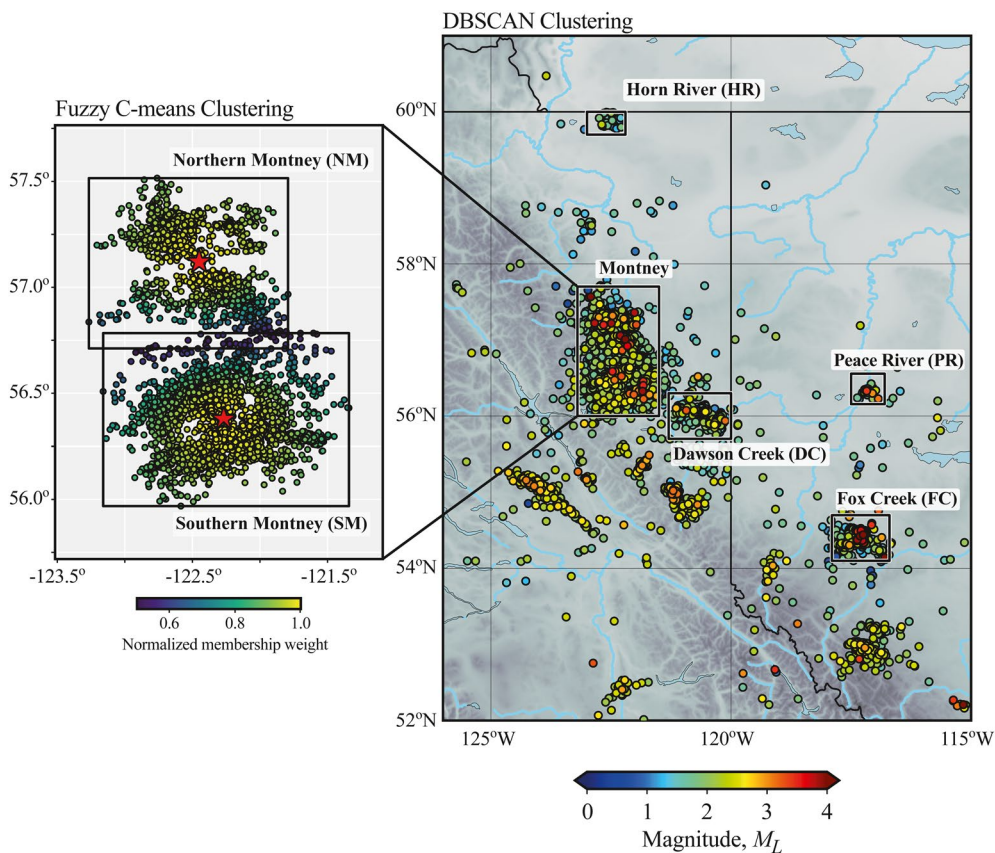


Figure 2. The seismicity clusters in western Canada obtained from DBSCAN. The inset shows the results of the Fuzzy C-means clustering algorithm and two subclusters of the Montney cluster (i.e., Northern Montney and Southern Montney). The red stars show the center of the North and South Montney clusters obtained from Fuzzy C-means. The injection-induced seismicity in western Canada is grouped into six major clusters: Peace River (PR), Fox Creek (FC), Dawson Creek (DC), South Montney (SM), North Montney (NM), and Horn River (HR).

These clusters are named according to their geographic locations as: PR (Peace River), FC (Fox Creek), DC (Dawson Creek), MBC (Montney Play of NE BC), and HR (Horn River). The remaining clusters are considered to be linked to quarry blasts and mining activities (Dokht et al., 2020; Fereidoni & Atkinson, 2017).

Spatiotemporal analysis of seismicity in the MBC cluster indicates an evident change in the rate of seismicity between the northern and southern segments of this cluster approximately 2 years after the beginning of the study period, though no significant variation in the cumulative injected fluid volume was observed among them (Figure S4). In the northern and southern segments, the seismicity levels are relatively higher during the first 2 years and the last year of the experiment, respectively (Figures S4a–S4e). The monthly distribution of injected fluid for the MBC cluster shows a concentration of large volume of HF fluid injected into $\sim 1.5\text{--}2.5$ km depths in the northern segment in 2014–2015 (Figures S5a–S5c), which gradually disappears toward the south (Figures S5d and S5e). Using the average (2.5 km) and standard deviation (2.3 km) of the major axis lengths of error ellipses of the events within the MBC cluster, DBSCAN is not able to divide this cluster into further subsets. To determine the boundary between the northern and southern segments of the Montney group, we rely on the Fuzzy C-means clustering algorithm (Bezdek et al., 1984), a form of clustering in which each event can belong to more than 1 cluster. This algorithm assigns cluster membership weights for each event, \mathbf{x}_i , by minimizing

$$J = \sum_{i=1}^n \sum_{j=1}^c \omega_{ij}^m \|\mathbf{x}_i - \mathbf{c}_j\|^2, \quad (1)$$

where \mathbf{c}_j is the center of the j th cluster and ω_{ij}^m is the membership weight of the i th event in the j th cluster which is defined as:

$$\omega_{ij}^m = \left(\sum_{k=1}^c \left(\frac{\|\mathbf{x}_i - \mathbf{c}_j\|^2}{\|\mathbf{x}_i - \mathbf{c}_k\|^2} \right)^{\frac{2}{m-1}} \right)^{-1}; m \geq 1. \quad (2)$$

Here, the parameter m determines the level of fuzziness and is commonly set to 2 (Frias-Martinez et al., 2006; Hashemzadeh et al., 2019). Setting the number of clusters to $c = 2$, the boundary between the two clusters (hereafter called NM for North Montney and SM for South Montney) coincides with the boundary observed from the spatiotemporal variation in the rate of seismicity (see Figures 2 and S4). Subsequently, the IIEs in western Canada can be grouped into six distinct clusters (the PR, FC, DC, SM, NM, and HR clusters; see Figure 2).

2.3. Frequency-Magnitude Distribution and Seismogenic Index (Σ)

To describe the relationship between seismicity and injected fluid volume, Shapiro et al. (2010) introduced the seismogenic index, Σ , which is modified from the classical Gutenberg-Richter relation to characterize the seismotectonic state of an injection site. For a nondecreasing injection pressure, the expected number of events with magnitudes larger than M after time t , $N_M(t)$, can be estimated as

$$\log_{10}[N_M(t)] = \log_{10}[Qc(t)] - \log_{10}[F_t S] + a - bM, \quad (3)$$

where $Qc(t)$ is the cumulative injected volume until time t , and a and b are the productivity parameter and slope of the Gutenberg-Richter distribution, respectively (Gutenberg & Richter, 1944). S is the poroelastic uniaxial storage coefficient related to porosity and F_t represents the tectonic potential controlling the level of seismicity in the injection region (Shapiro & Dinske, 2009). The term $a - \log_{10}[F_t S]$, known as the seismogenic index, Σ , is introduced independent of time and injection parameters and provides a means for predicting event magnitudes induced by fluid injection and their occurrence probabilities. The seismogenic index quantifies the number of induced events, within a specific magnitude range, for a unit volume of injected fluid (Langenbruch & Zoback, 2016). The larger the seismogenic index, the larger the probability of the occurrence of a significant magnitude earthquake (Dinske & Shapiro, 2013; Shapiro et al., 2010). Spatial variations in the seismogenic index give insight into the concentration of preexisting fractures and the state of stress at injection sites (Shapiro et al., 2010). In this study, we follow the procedure of Langenbruch & Zoback (2016) to investigate the effect of injection activity on enhanced seismicity for major clusters in western Canada and present seismogenic index models that average over all the physical properties within these broad regions.

3. Results

3.1. Frequency-Magnitude Distributions

In this study, the magnitude of completeness (M_C) was obtained from the point of maximum curvature of the frequency-magnitude distribution (Wiemer & Wyss, 2000) and the a - and b -values of the Gutenberg-Richter (GR) relation are estimated from the linear curve fitting using the least-squares method (Wiemer & McNutt, 1997). To estimate the confidence intervals of the GR relation parameters, we employ the bootstrap resampling technique (Efron, 1982; Schorlemmer et al., 2003) by drawing 200 replicates with replacement from the detected events in each cluster. The errors in the M_C estimates are given by the standard deviation of the bootstrapped samples.

The largest number of events have been recorded in the Montney clusters (SM with 1,544 and NM with 1,268 events; Table S2) followed, in descending order, by the DC (775 events) and FC (481 events) clusters. From the overall frequency-magnitude distributions of individual clusters, it was observed that the b -values range from 0.74 (in the FC cluster) to 1.6 (in the DC cluster) with an average value of 1.1 (Figure 3). This is slightly larger than the b -value of 0.97 estimated from the tectonic background seismicity recorded from

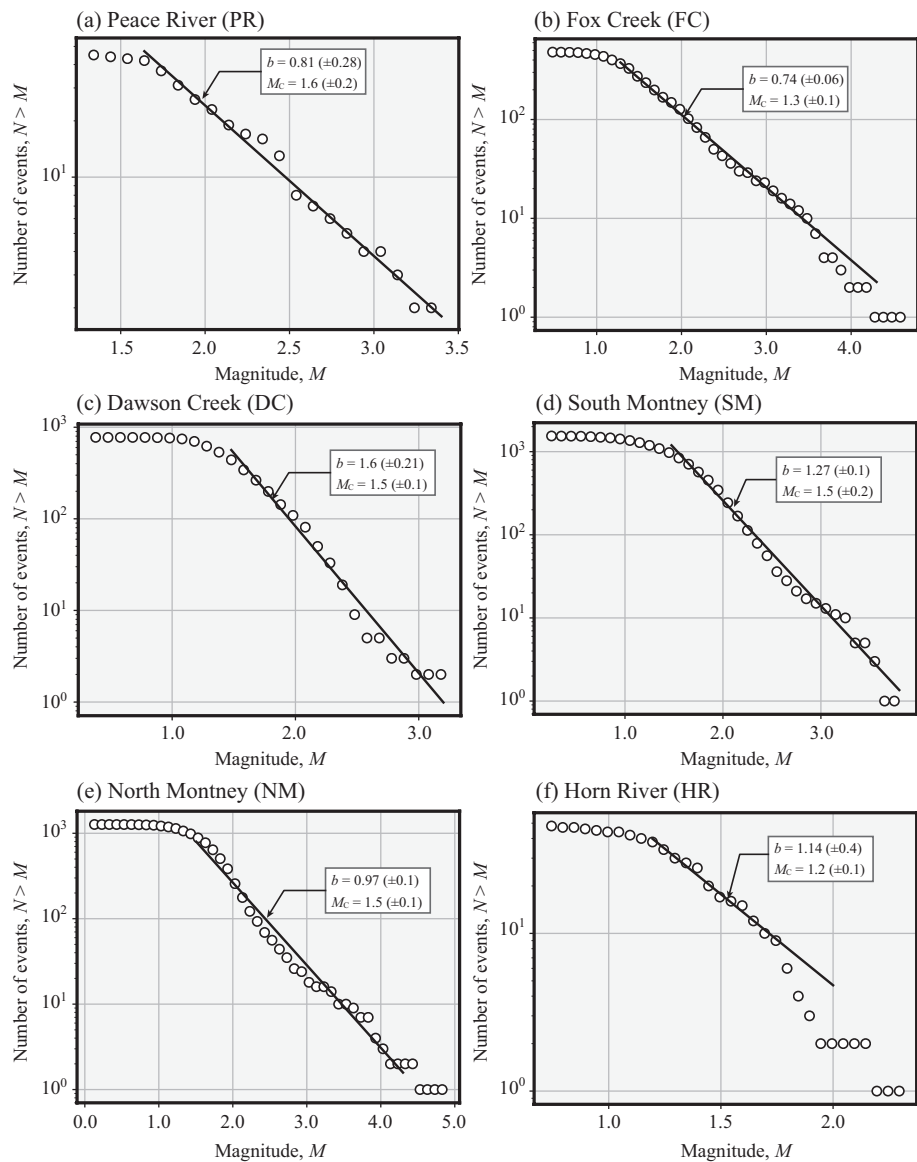


Figure 3. Earthquake frequency-magnitude distributions of the (a) Peace River, (b) Fox Creek, (c) Dawson Creek, (d) South Montney, (e) North Montney, and (f) Horn River clusters obtained from the entire seismic events recorded between January 2014 and December 2016. The solid black lines represent the estimated Gutenberg-Richter (GR) relationships. The b -value and magnitude of completeness (M_C) of the GR relation of each cluster are presented. The standard deviations of the b -value and M_C are obtained from bootstrap resampling with 200 replicates (Efron, 1982).

1964 to 1999, prior to a sudden increase in seismic activity in western Canada due to fluid injection operations (Figure S6). In comparison, the M_C shows less variation across the entire study area varying between 1.2 and 1.6 (see Figure 3), which is significantly smaller than the one obtained from the frequency-magnitude distribution of historic seismicity due to improvements in the seismic monitoring capacity (see Figure 1 and Table S1 for a list of active seismic stations during the study period). The largest uncertainties in the GR relation parameters are observed in the HR (b -value = 1.14 ± 0.4 and $M_C = 1.2 \pm 0.1$) and PR (b -value = 0.81 ± 0.28 and $M_C = 1.6 \pm 0.2$) clusters, the areas with the least number of seismic events (48 events in the HR cluster and 45 events in the PR cluster from 2014 to 2016).

Moreover, we investigate the annual variations in the frequency-magnitude distributions and the parameters of the GR relationships for each cluster if sufficient number of seismic events are available. The annual changes in the b -values in Fox Creek, Dawson Creek, and North Montney remain nearly insignificant

within the uncertainty limits of each cluster calculated from bootstrapping (Figure S7). On the other hand, in South Montney, the b -value gradually increases from 1.17 in 2014 to 1.76 in 2016 (see Figure S7c). The magnitudes of completeness, however, vary within the 95% confidence limits of the M_c values that were observed from the overall frequency-magnitude distributions of the entire time span (see Figures 3 and S7). It is worth mentioning that only one seismic event was recorded in Horn River after 2014 and the annual number of earthquakes recorded in Peace River is insufficient for further temporal analysis (see Table S2).

3.2. Seismogenic Response to Fluid Injection

In the WCSB, the spatial distributions of local seismicity and fluid injection volume demonstrate, on a large scale, a clear correlation between areas where high volumes of fluids have been injected and areas that have experienced an increase in seismic activity (Figure 4). In addition, in none of the investigated clusters, natural tectonic earthquakes show any spatial correlation with the occurrence of seismicity during the injection activity (Figures 4 and S8).

To identify the seismogenic wells, Rubinstein and Mahani (2015) suggest a distance threshold of 10 km between an induced earthquake and the closest injection point. Additionally, we account for the uncertainty in earthquake locations and establish an extended distance threshold by including the epicentral error in the spatial correlation analysis. In the next step, we employ a temporal filter and include only injection wells that have been active at least within a one-month time window prior to the occurrence of induced events. The one-month time window is chosen to be consistent with the temporal resolution of ER and WD injection data which have been reported on a monthly basis. Within the Montney Formation (i.e., the Fox Creek, Dawson Creek, South Montney, and North Montney clusters), more than 80% of the seismicity are found to be spatiotemporally linked to HF and the remaining IIEs are considered to be mostly associated with WD (see Table S3 and Figure S8). On the other hand, in Peace River and Horn River, the induced seismicity is entirely due to the disposal of waste fluid (see Figure S8).

The distributions of distances between each seismic event and the closest active injection well show median values of <6 km for most of the clusters (Figure S9). For the DC, SM, and NM clusters, the distributions are highly skewed toward zero and can be characterized by having a large excess kurtosis of greater than 5. The distribution for the FC cluster shows weak tails and is slightly skewed to the left with excess kurtosis of ~2. However, the peak values for all of the four clusters remain <2 km with most of the IIEs (~80% of the events) occurring in close proximity (≤ 5 km) to the closest well (see Figures S9b–S9e). On the contrary, the distributions for PR and HR more closely resemble a normal distribution with excess kurtosis of nearly equal to 0 and the majority of events in these two clusters are located at large distances (≥ 10 km) from the closest well (Figures S9a and S9f). Due to the sparse station coverage in the area during the study period, for which the injection data were available, the earthquake depths cannot be accurately determined and 15–32% of the events in different clusters have been located using a fixed depth of 1 km (Figure S10). This hinders us from further investigating the correlation between the earthquake and injection depths.

In general, the temporal distributions of local seismicity and cumulative injected fluid volume demonstrate changes in the rate of seismicity in response to temporal changes in injection rate (Figures S11 and S12). In Fox Creek, Dawson Creek, and North Montney, where HF-induced events are dominant, an increase in the rate of HF injection is followed by a sharp increase in seismic activity over a broad magnitude range (Figures S11b, S11c, and S11e). On the other hand, in South Montney, the variation of earthquake magnitudes as a function of the cumulative injected volume becomes more homogeneous (i.e., a significant level of seismicity is still observed during periods of relatively low injection rate; see Figures S11d and S12d). In Horn River, the seismicity ceased in early 2015 after the monthly WD injection rate sharply decreased and remained significantly low until the end of our study period (see Figure S11f).

Before 1999, the historic earthquake catalog of western Canada, compiled by the Canadian National Earthquake Database, indicates an average of one event with magnitude greater than 1.5 per year. In recent years, the comprehensive catalog of induced seismicity documents a significant increase in the number of M_L or $M_W \geq 1.5$ earthquakes in the study region with an annual average of 5 (in Horn River) to 286 (in North Montney) events (see Table S4). For the recorded seismicity above the detection threshold of 1.5, there is a significant correlation between the cumulative number of seismic events and cumulative injected fluid volume

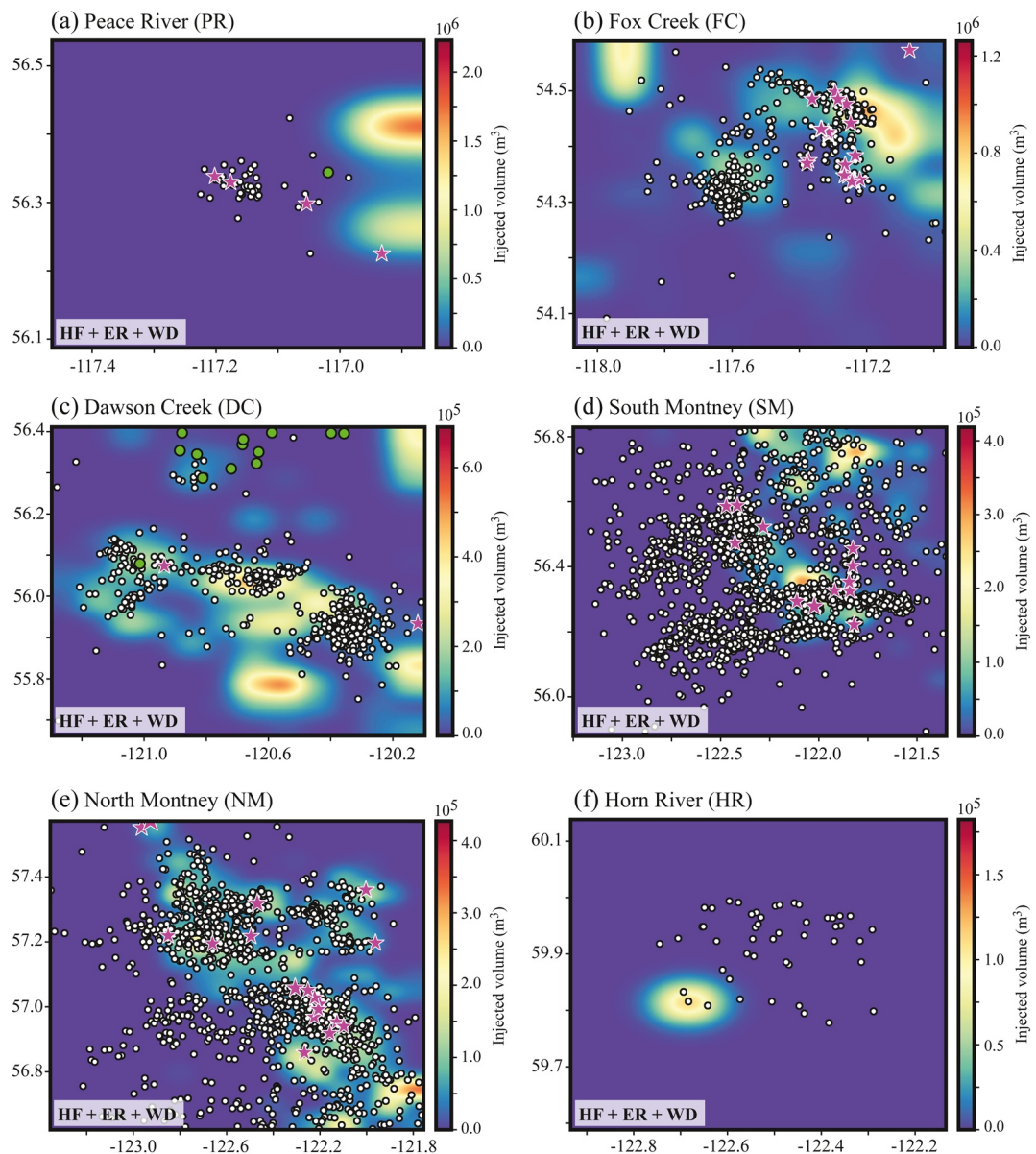


Figure 4. Total injected volume of the hydraulic fracturing (HF), enhanced recovery (ER) and wastewater disposal (WD) fluids for the (a) Peace River (PR), (b) Fox Creek (FC), (c) Dawson Creek (DC), (d) South Montney (SM), (e) North Montney (NM), and (f) Horn River (HR) clusters, stacked in grid cells of 0.05° latitude-by- 0.1° longitude. The green circles represent earthquakes recorded between 1964 and 1999 (obtained from the Canadian National Earthquake Database). The white circles show the local seismicity cataloged by the Geological Survey of Canada between 2014 and 2016. The pink stars represent earthquakes with magnitude $M_L \geq 3$ in the catalog.

in all clusters (Figure 5), with the square of the correlation coefficient, R^2 , varying from 0.67 (in Horn River) to 0.98 (in South Montney). Using the estimated b -values for the entire injection duration and a magnitude cutoff of 1.5, the Σ values can be derived to qualitatively compare the seismic hazard potential between different clusters. After a short injection period and recording a sufficient number of events of significant magnitudes (equal to or above the cutoff magnitude of 1.5), it can be observed that the temporal variation in Σ becomes relatively stable and remains nearly constant (Figure S13). Temporal lags between sudden increases in injection rate and seismicity manifest themselves as deviations from the linear dependence of the cumulative number of induced events on the cumulative injected volume (see Figures S11 and S13). The calculated Σ at the end of the study period falls approximately within the 95% confidence interval of

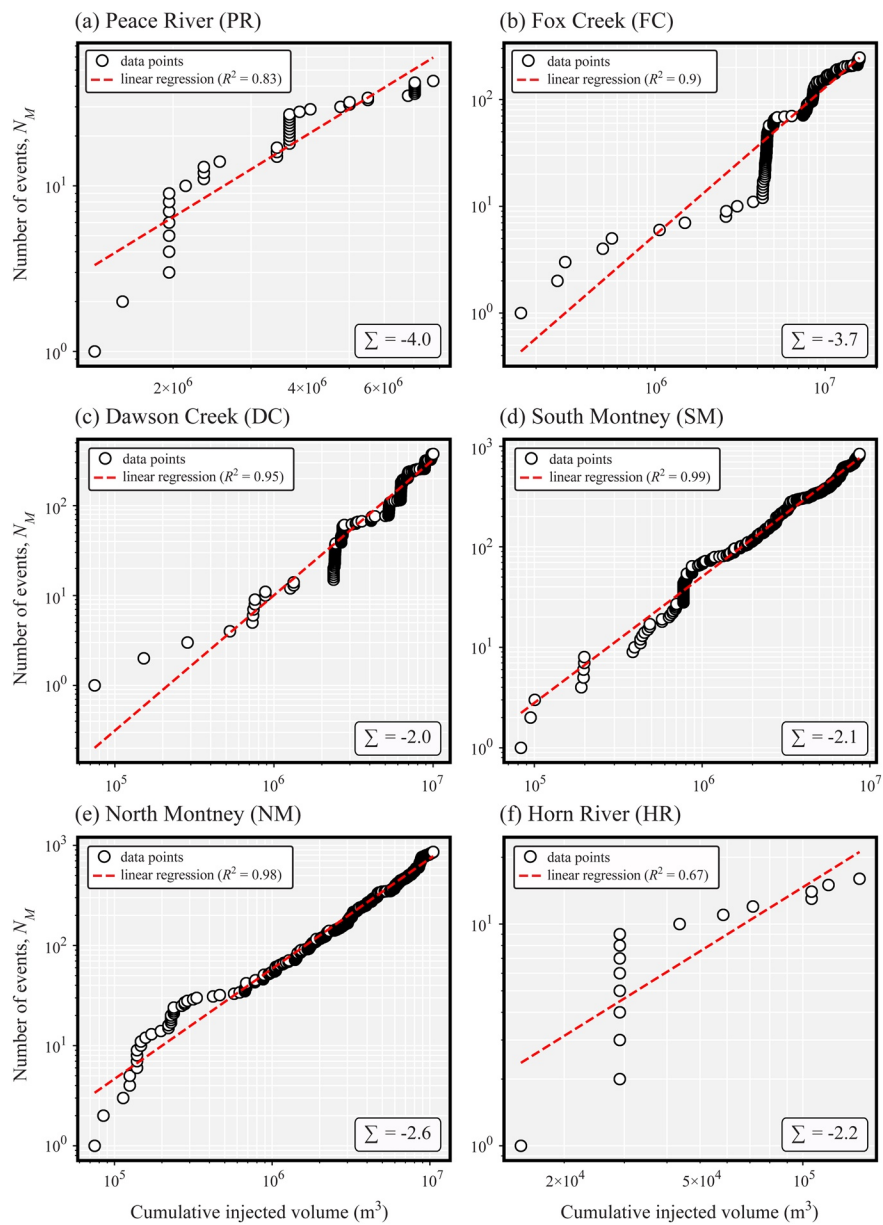


Figure 5. The number of events with magnitude larger than 1.5 as a function of cumulative injected fluid volume for the (a) Peace River, (b) Fox Creek, (c) Dawson Creek, (d) South Montney, (e) North Montney, and (f) Horn River clusters in the log-log scale. The square of the correlation coefficient (R^2) of the least-squares regression fit (dashed line) and seismogenic index of the entire injection duration (Σ) for each individual cluster are presented.

its average value in each cluster (see Figures 5 and S13). The final Σ values vary from -4.0 to -1.8 , with the largest and smallest indices obtained for the Dawson Creek and Peace River clusters, respectively. The calculated Σ indices can be further employed to estimate the occurrence probabilities of earthquakes potentially induced by deep fluid injection.

4. Discussion

The potential connection between the recorded seismic events and injection activities forms the basis of our analysis of the seismotectonic state of the clustered injection sites and further seismic hazard assessments in western Canada. The spatiotemporal distributions of seismicity and injection wells indicate the presence

of induced events at distances up to ~40 km from the injection points (see Figure S9). Previous observations have shown that seismicity can be induced over an extensive spatial range from the wells (Goebel et al., 2015; Hsieh & Bredehoeft, 1981; Keranen et al., 2014; Rubinstein & Mahani, 2015), where the continued propagation of the pressure front and the resulting poroelastic stress perturbations can potentially intensify the seismogenic response in the far-field of high-rate injection wells (Goebel et al., 2017; Healy et al., 1968). However, the presence of IIEs at relatively large distances from injection points, especially for HF-induced seismicity, remains a topic of debate that deserves further investigation (Schultz et al., 2020).

A recent study by Dokht et al. (2020) on blasting-induced events in central BC shows that the reported location errors in the original catalog can be underestimated if the station coverage is suboptimal and the uncertainties in the velocity model are not taken into account. To verify the robustness of the observed seismicity at great distances from the corresponding injection sites, we obtain the probabilistic earthquake hypocenters using a three-dimensional Oct-Tree implementation of the NonLinear Location (NonLinLoc) algorithm (Lomax et al., 2000; see Table S5 for a set of parameters used in NonLinLoc). The resulting probability density functions of the hypocentral locations allow us to estimate the largest location uncertainty caused by errors both in the picked and theoretical arrival times. Requiring the events to have at least five picks, the obtained results from the 68% confidence ellipses show an average location error varying from 3.5 km (in DC) to ~9 km (in HR). The average length of the semimajor axes of the error ellipses can be as large as nearly 10 km for the SM, NM, and HR clusters (Figure S14). The results of the nonlinear uncertainty analysis stress the importance of taking the earthquake location error into account when investigating the occurrence of IIEs at great distances from an injection point.

The highest likelihood zones of seismic activity, calculated from stacking the scattered clouds of individual nonlinear solutions, depict the significance of the correlation between the local seismicity and the lateral extent of the corresponding injection activity (Figure 6). In Fox Creek, Dawson Creek, South Montney, and North Montney, the zones with the highest density of scatter samples are enclosed within the approximate boundaries of HF injection (especially within the Fox Creek and North Montney clusters; see Figures 6b–6e). On the other hand, in Peace River and Horn River, the highest likelihood zones of induced seismicity fall in the vicinity of the extent of WD injection (see Figures 6a and 6f).

The availability of a comprehensive earthquake catalog enables us to obtain reliable estimates of the GR relation parameters in regions of clustered seismicity. The *b*-values obtained in the present research fall within the same range of values observed in earlier studies in the same areas (Farahbod et al., 2015; Roth et al., 2020; Schultz et al., 2018). Relatively smaller *b*-values in FC and NM correspond to the more frequent occurrence of larger events ($M_L \geq 3.5$) within the two clusters compared to other regions in western Canada (see Figures 3b and 3e), which may be an indication of preexisting fault reactivation due to fluid injection (Davies et al., 2013; Maxwell et al., 2009).

The seismogenic indices obtained in this study are in excellent agreement with the previously reported values, ranging from -4 to -1.5, for the HF and WD sites in central AB and northern BC (Bao & Eaton, 2016; Hajati et al., 2015; Schultz et al., 2014; Verdon & Budge, 2018). To investigate the possible contribution of injected volume from aseismic HF wells to the estimated seismogenic responses, we use temporal filters of shorter lengths and measure changes in the overall seismogenic indices. Although, as expected, slightly larger seismogenic indices are obtained in Fox Creek, Dawson Creek, South Montney, and North Montney due to reduction in the cumulative injected volume using shorter time windows, the observed changes remain insignificant and do not exceed one standard deviation of the average Σ values (see Table S6 and Figure S13).

Furthermore, to evaluate the sensitivity of the seismogenic index to changes in the cutoff magnitude, we adjust the cutoff magnitude for each cluster to the magnitude of completeness of the corresponding GR relationship. Considering the combined effect of the cutoff magnitude and the total number of induced events with magnitudes above the completeness threshold (see Equation 3), a slight increase or decrease in cutoff magnitude has a negligible effect on the resulting Σ value. Thus, the approach of estimating seismogenic indices with a unified cutoff magnitude remains valid (see Table S7).

The estimated Σ values provide us a means to compare the seismotectonic state at different injection sites and different times. Several previous studies have been conducted to determine the physical mechanism

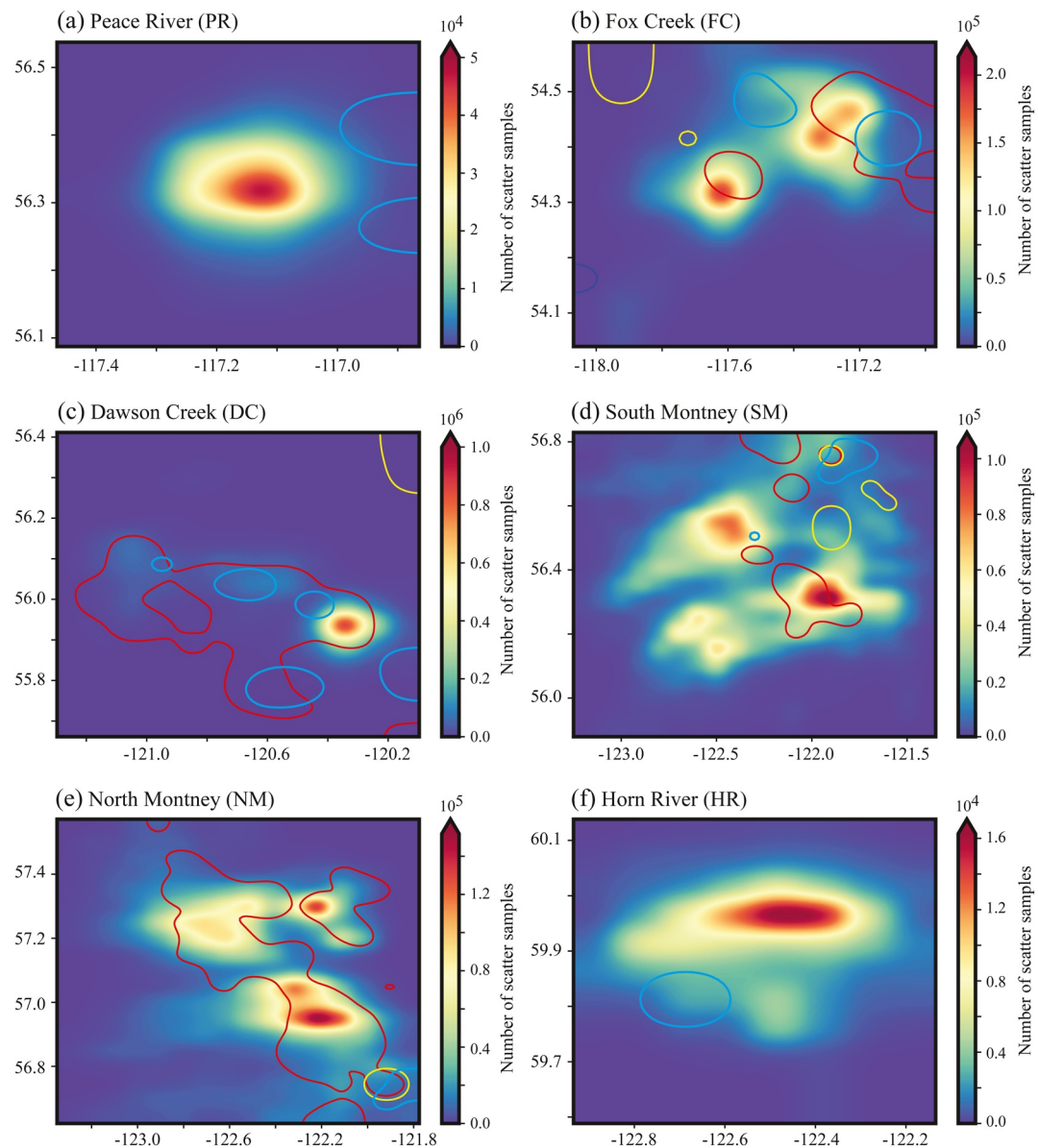


Figure 6. Maps of the stacked scatter clouds obtained from the NonLinLoc solutions for the (a) Peace River, (b) Fox Creek, (c) Dawson Creek, (d) South Montney, (e) North Montney, and (f) Horn River clusters. The scatter points are stacked in grid cells of 0.05° latitude-by- 0.1° longitude and smoothed using a Gaussian kernel. The red, yellow, and blue contours mark the approximate boundaries of the HF, ER, and WD injections, respectively. The extent of each injection type is determined at the 20% level of the maximum value of the corresponding gridded injection volume shown in Figure S8. The 20% level is selected to aid visual interpretation of the spatial correlation between seismicity and injection activity.

responsible for fluid injection-induced seismicity. Recent studies suggest that the occurrence of seismic events of significant magnitudes responds to perturbations in the local stress field in a reservoir associated with abrupt changes in injection rates (Barbour et al., 2017; Martínez-Garzón et al., 2014; Norbeck & Rubinstein, 2018; Weingarten et al., 2015). In this study, we consider injected-related seismicity at six different major clusters in western Canada during a nondecreasing injection flow rate period for most of the clusters (except North Montney; Figure S15). Significant magnitude events, especially in Fox Creek, Dawson Creek, South Montney, and North Montney, are found to be preceded by an overall increase in injection rate (see Figures S11 and S15). Difficulties associated with nonuniform station coverage and large location

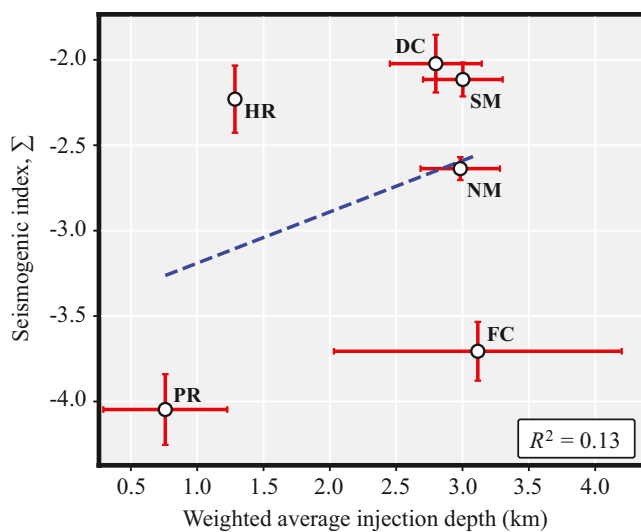


Figure 7. Variation in the seismogenic index with respect to the weighted average injection depth. The square of the correlation coefficient (R^2) of the least-squares regression fit (dashed blue line) is presented. The error bars represent one standard deviation from the estimated seismogenic index and average injection depth at the end of the study period.

depth of ~ 3 km; Figures 7 and S16). The limited number of measurements prevents us from drawing a robust conclusion; however, the overall trend appears to be consistent with increasing shear strength of rocks with depth which assists the occurrence of significant earthquakes (Dinske & Shapiro, 2013).

Kao, Hyndman, et al. (2018) suggested that the tectonic moment rate, in addition to the total injected volume, governs the spatial distribution of IIEs in western Canada. A NW-SE trending band of high levels of seismicity and injection volume (Figure 1) was found to be consistent with the overall pattern of the isostrain rate contours (Figure 8a) and overlaps with a zone of moderate tectonic moment rates (Figure 8b) ranging $8-22 \times 10^5 \text{ Nm/m}^2/\text{year}$ (readers are referred to Kao, Hyndman, et al. (2018) for a detailed discussion on the estimation of the tectonic moment rate). Statistically, there is a strong positive correlation between the seismogenic index and the level of tectonic activity ($R^2 > 0.7$; Figure 9). The largest Σ values are observed within the Horn River Basin and Montney Formation of BC, where the tectonic moment rate is on the order of $\sim 20 \times 10^5 \text{ Nm/m}^2/\text{year}$; however, the cumulative injected volume is not essentially the largest (see Figures 9, S11, and S12). The lack of induced seismicity in the easternmost segment of the study area, in spite of large injection volumes (see Figure S1), was suggested to be due to low tectonic moment rates of $< 10^6 \text{ Nm/m}^2/\text{year}$ (see Figure 9; Kao, Hyndman, et al., 2018). These observations emphasize the necessity of considering the effects of other controlling factors in investigating the underlying cause of injection-induced seismicity as concluded in previous studies (Amini & Eberhardt, 2019; Brodsky & Lajoie, 2013; Hincks et al., 2018; Pei et al., 2018; Schultz et al., 2018).

To measure the relationship between the seismic moment released from local earthquakes, ΣM_0 , and theoretical strain energy introduced by injection, Hallo et al. (2014) introduced a seismic efficiency ratio, S_{EFF} :

$$S_{\text{EFF}} = \frac{\Sigma M_0}{\mu \Delta V}, \quad (4)$$

where μ is the rock shear modulus (assumed to be 30 GPa; Kao, Hyndman, et al., 2018) and ΔV is the cumulative injected volume. Regardless of differences in area size and activity time duration among the clusters, the estimated seismic efficiency provides a means to investigate if the injection-introduced strain has been fully released seismically. For S_{EFF} greater than 1, the seismic energy is considered to exceed the energy bound by the injection, suggesting that induced earthquakes release the tectonically accumulated strain energy (Verdon & Budge, 2018). Similar to the temporal variation in the seismogenic index (Figure S13),

uncertainty and the limited temporal resolution of WD and ER injection data prevent us from a consistent analysis of the effects of varying injection rates across different clusters.

To investigate the relationship between the seismogenic activation potential and reservoir depth in the study area, we calculate the weighted average injection depth in each cluster as an approximation to the reservoir depth using the injection parameters compiled in our database (Figure S16). Within the WCSB in central AB, the injection depth was found to be one of the dominant controlling factors on the reactivation of preexisting basement-rooted faults and proliferation of induced events (Pawley et al., 2018; Schultz et al., 2016; Wang et al., 2017). Recent studies on the HF-induced seismicity in the Montney Formation of NE BC indicate that the majority of induced earthquakes with smaller magnitudes occurred slightly above the injection horizons within the sedimentary layers (Peña Castro et al., 2020; Roth et al., 2020; Yu et al., 2019). In the present study, the seismogenic index shows a weak positive correlation with the weighted average injection depth ($R^2 = 0.13$; Figure 7). The average injection depth in Fox Creek shows a large standard deviation due to a significant volume of waste fluid injected at shallow depths (see Figure S16b). The smallest Σ value corresponds to the Peace River cluster with the shallowest average injection depth (< 1 km). Generally, the largest Σ values are observed for the clusters within the Montney Formation of NE BC associated with large injection volumes at relatively greater depths (an average

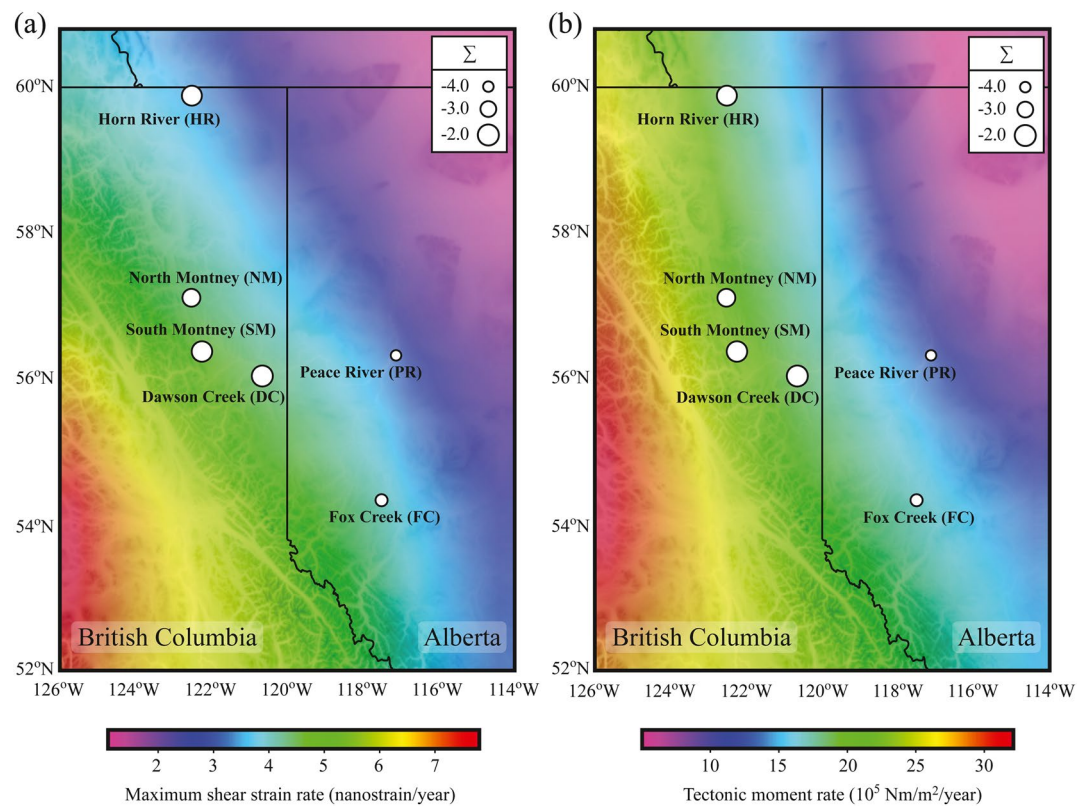


Figure 8. Distributions of the (a) maximum shear strain rate and (b) tectonic moment rate estimated from maximum horizontal strain rate and the thickness of the seismogenic layer (see Kao, Hyndman, et al., 2018, for details). The white circles mark the locations of the six clusters investigated in this study. The induced seismicity in western Canada is mostly limited to a zone of moderate tectonic moment rate of $\sim 10\text{--}20 \times 10^5$ Nm/m²/year and relatively high injection volume (see Figures S1 and S8). The tectonic moment rates are calculated using a shear modulus of 30 GPa.

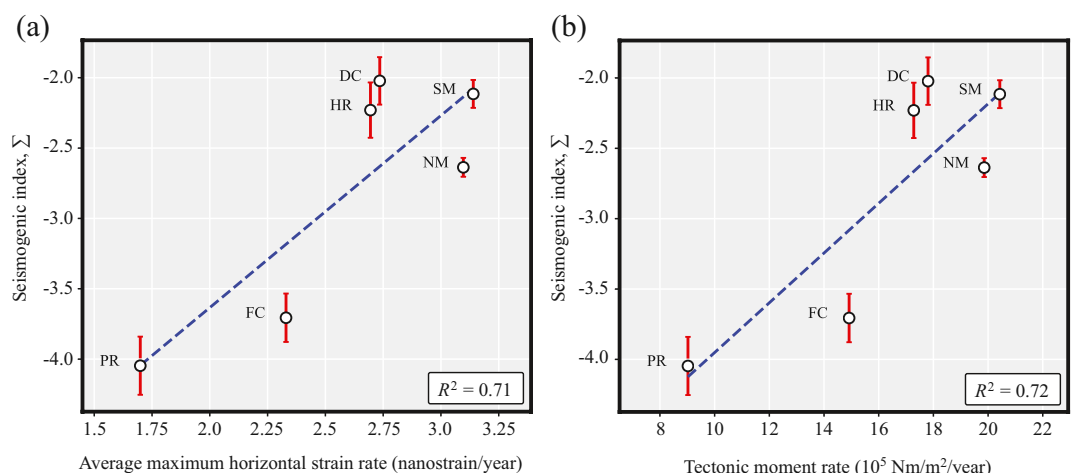


Figure 9. Variation in the seismogenic index as a function of the (a) average maximum horizontal strain rate and (b) tectonic moment rate. The square of the correlation coefficient (R^2) of the least-squares regression fit (dashed blue line) is presented. The error bars show one standard deviation from the estimated seismogenic index at the end of the study period.

Table 1
Summary of a Comparative Analysis of the Seismotectonic State of the Clusters

Location	Days	Injection volume (m^3)			Σ		$\log_{10}(S_{\text{EFF}})$	
		HF	ER	WD	Average	Cumulative	Average	Cumulative
PR	899	0	6.8×10^4	7.7×10^6	$-4.1(\pm 0.2)$	-4.0	$-2.5(\pm 0.1)$	-2.6
FC	1,083	9.4×10^6	3.3×10^6	3.2×10^6	$-3.8(\pm 0.2)$	-3.4	$-1.7(\pm 0.2)$	-1.4
DC	1,057	6.5×10^6	4.7×10^5	3.0×10^6	$-2.2(\pm 0.2)$	-1.8	$-2.8(\pm 0.1)$	-2.7
SM	1,088	6.4×10^6	9.9×10^5	1.3×10^6	$-2.2(\pm 0.1)$	-2.0	$-1.9(\pm 0.2)$	-1.9
NM	1,094	8.2×10^6	8.9×10^5	1.4×10^6	$-2.7(\pm 0.1)$	-2.6	$-1.1(\pm 0.5)$	-0.8
HR	353	0	0	1.5×10^5	$-2.1(\pm 0.2)$	-2.2	$-2.4(\pm 0.2)$	-2.4

Note: The cumulative seismogenic index and seismic efficiency ratio refer to the values obtained at the end of the study period.

Abbreviations: DC, Dawson Creek; FC, Fox Creek; HR, Horn River; NM, North Montney; PR, Peace River; SM, South Montney.

the S_{EFF} ratio is observed to become stable quickly and varies within one standard deviation of its mean for most of the clusters (Figure S17). It was also found by Verdon & Budge (2018) that the seismogenic index and seismic efficiency ratio follow the same trend as the cumulative moment release and the total number of events both scale linearly with injection volume (Clarke et al., 2019; Van der Elst et al., 2016). The estimated S_{EFF} ratios remain <1 for the entire clusters with $\log_{10}(S_{\text{EFF}})$ ranging from -0.8 to -2.7 at the end of the study period (Table 1 provides a comparison between the S_{EFF} ratios among different clusters). These observations are in excellent agreement with the previously reported S_{EFF} ratios for the hydraulic fracturing and saltwater disposal sites (cf. Table 2 in Hallo et al., 2014).

Once the seismic efficiency is determined, the maximum magnitude of an induced earthquake that will not be exceeded during injection activity can be estimated using the injection-introduced strain energy. Assuming that the S_{EFF} ratio and the b -value of the GR distribution do not vary significantly with time, the largest expected event magnitude can be calculated as (Clarke et al., 2019):

$$M_{\text{Max}}^{S_{\text{EFF}}} = \frac{2}{3} \left(\log_{10} \left(\frac{S_{\text{EFF}} \mu \Delta V (1.5 - b)}{b 10^{9.1}} \right) + \log_{10} \left(10^{b\delta} - 10^{-b\delta} \right) \right), \quad (5)$$

where δ is the probabilistic half-bin size defined around the maximum magnitude in the GR distribution (Hallo et al., 2014). In comparison with the forecasts of $M_{\text{Max}}^{S_{\text{EFF}}}$, the method of Shapiro et al. (2010) provides a solution for the largest magnitude that may be induced in a probabilistic sense:

$$M_{\text{Max}}^{\Sigma} = \frac{\Sigma - \log_{10} \left(\frac{-\ln(\chi)}{\Delta V} \right)}{b}, \quad (6)$$

in which χ determines the upper limit for M_{Max}^{Σ} at a given confidence level (Verdon & Budge, 2018).

To estimate the temporal variations in $M_{\text{Max}}^{S_{\text{EFF}}}$ and M_{Max}^{Σ} over the injection period, we continuously update the S_{EFF} ratio and Σ index of individual clusters using a one-month time window (comparable to the temporal resolution of the WD and ER data) preceding each event (Figure 10). To accommodate uncertainties in the forecast and provide a conservative estimation of $M_{\text{Max}}^{S_{\text{EFF}}}$ that will not be exceeded, Verdon and Budge (2018) suggest applying a correction magnitude obtained from the comparison between the modeled and the largest sampled magnitudes drawn from synthetically generated event populations. However, we observe that the uncorrected magnitudes estimated from the S_{EFF} ratios, $M_{\text{Max}}^{S_{\text{EFF}}}$, are generally equal to or greater than the observed magnitudes in the study area (especially for large events; Figure 11). On the other hand, the forecasts of M_{Max}^{Σ} at the 68% confidence level (hereafter called $M_{\text{Max}}^{\Sigma 68}$) underestimate the lower bound of the magnitude envelope which is expected not to be exceeded during injection (Figures 10 and 11b). In

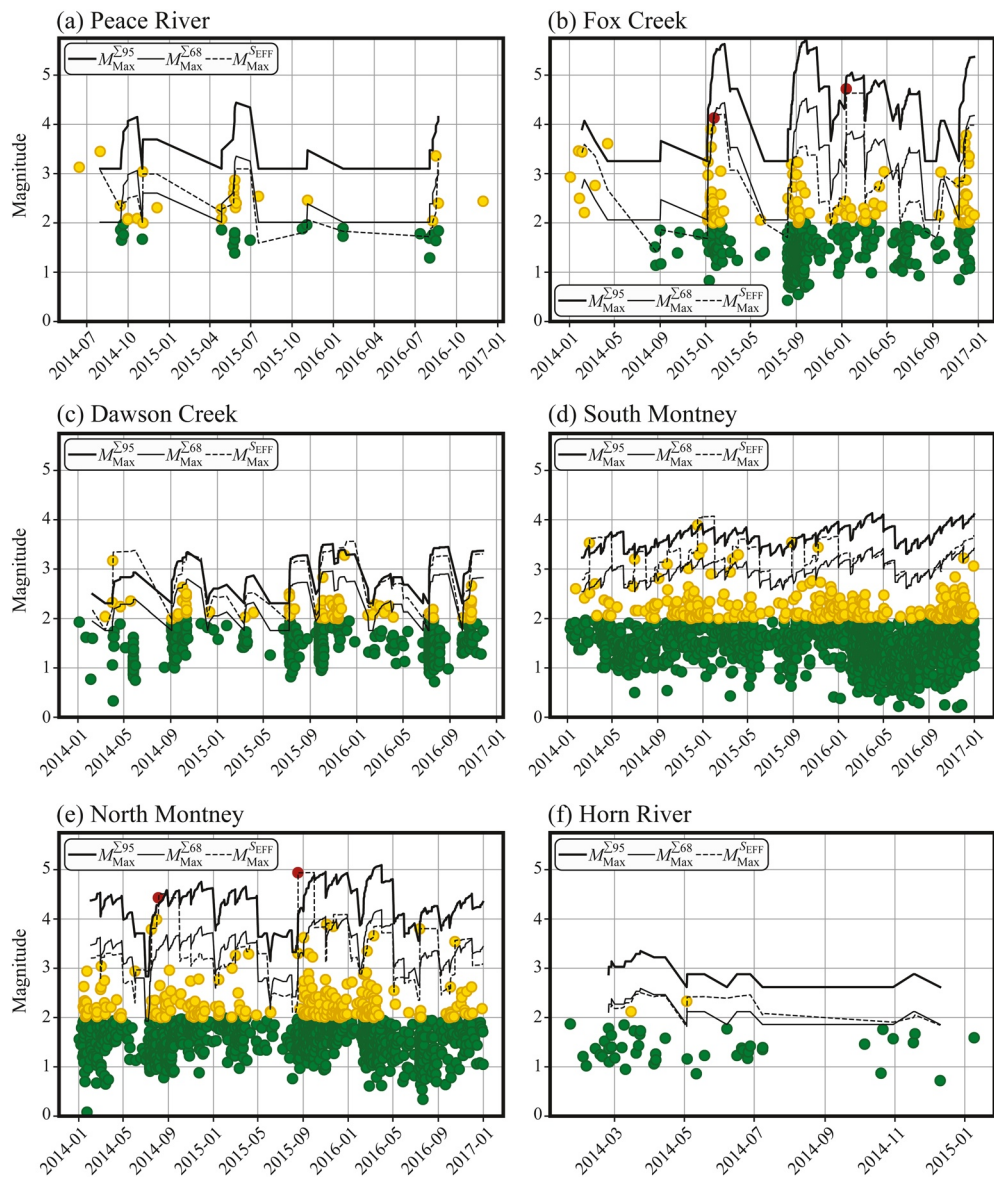


Figure 10. Forecasting the largest expected event size as a function of time using the seismic efficiency ratio ($M_{\text{Max}}^{\text{SEFF}}$: dashed lines), and seismogenic index (estimated at the 68% confidence level, $M_{\text{Max}}^{\Sigma 68}$: thin solid line, and estimated at the 95% confidence level, $M_{\text{Max}}^{\Sigma 95}$: thick solid line), and a sliding window length of 1 month for (a) Peace River, (b) Fox Creek, (c) Dawson Creek, (d) South Montney, (e) North Montney, and (f) Horn River. The green, yellow and red circles correspond to the Alberta Energy Regulator traffic light protocol cutoffs (Alberta Energy Regulator, 2015); green: $M_L < 2$; yellow: $2 \leq M_L < 4$; red: $M_L \geq 4$.

comparison, the lower bound of the M_{Max}^{Σ} forecasts at the 95% confidence level (hereafter called $M_{\text{Max}}^{\Sigma 95}$) provides a better estimation of the largest observed magnitudes. The correlation analysis between the observed and modeled magnitudes shows average errors of 0.3 (± 0.4), 0.3 (± 0.5), and 0.9 (± 0.5) for the $M_{\text{Max}}^{\text{SEFF}}$, $M_{\text{Max}}^{\Sigma 68}$ and $M_{\text{Max}}^{\Sigma 95}$ forecasts, respectively (see Figure 11a). These measurements are in good quantitative agreement with the previous forecasts for the magnitudes of the largest expected IIEs (Clarke et al., 2019; Van der Elst et al., 2016; Verdon & Budge, 2018; Verdon & Stork, 2016). Clarke et al. (2019) emphasize the importance of considering the cumulative effects of the injection volume and seismicity to avoid possible underestimation of the expected event magnitude. However, we observe that both approaches yield the same approximation for large events ($M \geq 4$; Figures 10 and S18).

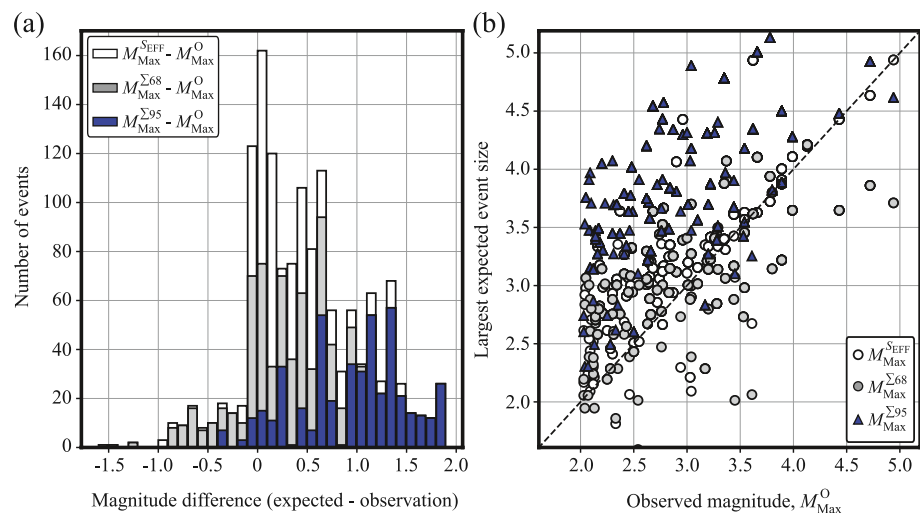


Figure 11. (a) Distributions of difference between the largest event magnitude observed in each month, $M_{\text{Max}}^{\text{O}}$, and the corresponding largest expected event magnitude estimated using the seismic efficiency ratio ($M_{\text{Max}}^{\text{EFF}}$: white bars), and seismogenic index (estimated at the 68% confidence level, $M_{\text{Max}}^{\Sigma 68}$: gray bars, and estimated at the 95% confidence level, $M_{\text{Max}}^{\Sigma 95}$: blue bars). (b) A scatter plot of estimated largest event magnitude with respect to the observed event magnitude.

5. Conclusions

An increasing occurrence trend of red-light injection-induced events ($M \geq 4$) in western Canada has raised significant concerns about the potential seismic hazard associated with the development of unconventional hydrocarbons. We perform a clustering analysis to investigate the spatiotemporal characteristics of regions of induced seismicity in association with broadly distributed injection in the Western Canada Sedimentary Basin. Spatial clusters are determined from the Density-Based Spatial Clustering of Applications with Noise and Fuzzy C-means algorithms based on the epicentral distance between the neighboring events and the location errors reported in the original catalog. The clusters are found to be colocated with areas of relatively high cumulative volume of injection and tectonic moment rates. The temporal analysis of the frequency-magnitude distributions shows that the annual changes in the b -values of the Gutenberg-Richter distributions remain insignificant for most of the clusters over the study period. The comparative analysis of spatial variations in the rate of seismicity with respect to the injection volume indicates that the seismogenic index varies between -4 and -2 across the study area. Generally, the seismicity clusters in northeastern British Columbia yield slightly larger estimates of the seismogenic index compared to those in western Alberta. The statistical models based on the estimated seismogenic indices are employed to forecast the magnitudes of the largest expected events induced during fluid injection. Thus, the present study has implications for regional seismic hazard assessments. Furthermore, an improvement in the local earthquake detection capabilities and availability of injection data in real time will assist both regulators and operators to mitigate the risk associated with induced seismicity.

Data Availability Statement

The Canadian National Earthquake Database catalog can be obtained from <https://earthquakescanada.nrcan.gc.ca> (last accessed in March 2021). The regional earthquake catalog used in this study was compiled by Natural Resources Canada (<https://doi.org/10.4095/306292>, last accessed March 2021) using the Antelope software package produced by Boulder Real Time Technologies. The database of injection wells from January 2014 to December 2016 was obtained using geoSCOUT (geoLOGIC systems Ltd.) licensed to Geoscience BC. DBSCAN and Fuzzy C-means clustering has been performed using the Clustering package in Julia. This is Natural Resources Canada (NRCan) contribution number 20200746.

Acknowledgments

The authors would like to thank the Editor Dr. Rachel Abercrombie, the Associate Editor, Ryan Schultz, and one anonymous reviewer for helpful comments and constructive reviews. This study was supported by the Environmental Geoscience Program of NRCan, NSERC, and Geoscience BC. This is Natural Resources Canada (NRCan) contribution number 20200746.

References

- Alberta Energy Regulator. (2015). *Subsurface order no. 2: Monitoring and reporting of seismicity in the vicinity of hydraulic fracturing operations in the Duvernay zone, Fox Creek, Alberta. AER Bulletin 2015-07*, 3. Retrieved from <https://static.aer.ca/prd/documents/bulletins/Bulletin-2015-07.pdf>
- Amini, A., & Eberhardt, E. (2019). Influence of tectonic stress regime on the magnitude distribution of induced seismicity events related to hydraulic fracturing. *Journal of Petroleum Science and Engineering*, 182, 106284. <https://doi.org/10.1016/j.petrol.2019.106284>
- Anderson, Z., & Eaton, D. W. (2016). Induced seismicity due to wastewater injection near Peace River, Alberta. In *GeoConvention*. Calgary, Canada
- Arlia, D., & Coppola, M. (2001). Experiments in parallel clustering with DBSCAN. In *European Conference on Parallel Processing* (pp. 326–331). Berlin, Heidelberg: Springer.
- Atkinson, G. M., Eaton, D. W., Ghofrani, H., Walker, D., Cheadle, B., Schultz, R., et al. (2016). Hydraulic fracturing and seismicity in the Western Canada Sedimentary Basin. *Seismological Research Letters*, 87(3), 631–647. <https://doi.org/10.1785/0220150263>
- Babaie Mahani, A., Kao, H., Atkinson, G. M., Assatourians, K., Addo, K., & Liu, Y. (2019). Ground-motion characteristics of the 30 November 2018 injection-induced earthquake sequence in Northeast British Columbia, Canada. *Seismological Research Letters*, 90(4), 1457–1467.
- Babaie Mahani, A., Schultz, R., Kao, H., Walker, D., Johnson, J., & Salas, C. (2017). Fluid injection and seismic activity in the Northern Montney Play, British Columbia, Canada, with special reference to the 17 August 2015 Mw 4.6 induced earthquake. *Bulletin of the Seismological Society of America*, 107(2), 542–552. <https://doi.org/10.1785/0120160175>
- Bao, X., & Eaton, D. W. (2016). Fault activation by hydraulic fracturing in western Canada. *Science*, 354(6318), 1406–1409. <https://doi.org/10.1126/science.aag2583>
- Barbour, A. J., Norbeck, J. H., & Rubinstein, J. L. (2017). The effects of varying injection rates in Osage County, Oklahoma, on the 2016 Mw 5.8 Pawnee earthquake. *Seismological Research Letters*, 88(4), 1040–1053. <https://doi.org/10.1785/0220170003>
- BC Oil & Gas Commission. (2012). *Investigation of observed seismicity in the Horn River basin (Tech. Rep.)*. Fort St. John, Canada:BC Oil and Gas Commission. Retrieved from <http://www.bcogc.ca/node/8046/download>
- Bezdek, J. C., Ehrlich, R., & Full, W. (1984). FCM: The fuzzy c-means clustering algorithm. *Computers and Geosciences*, 10(2–3), 191–203. [https://doi.org/10.1016/0098-3044\(84\)90020-7](https://doi.org/10.1016/0098-3044(84)90020-7)
- Borah, B., & Bhattacharyya, D. K. (2004). An improved sampling-based DBSCAN for large spatial databases. In *Proceedings of International Conference on Intelligent Sensing and Information Processing, 2004* (pp. 92–96).
- Brodsky, E. E., & Lajoie, L. J. (2013). Anthropogenic seismicity rates and operational parameters at the Salton Sea Geothermal Field. *Science*, 341(6145), 543–546. <https://doi.org/10.1126/science.1239213>
- Chopra, S., Sharma, R. K., Ray, A. K., Nemati, H., Morin, R., Schulte, B., & D'Amico, D. (2017). Seismic reservoir characterization of Duvernay shale with quantitative interpretation and induced seismicity considerations—A case study. *Interpretation*, 5(2), T185–T197. <https://doi.org/10.1190/int-2016-0130.1>
- Clarke, H., Verdon, J. P., Kettley, T., Baird, A. F., & Kendall, J.-M. (2019). Real-time imaging, forecasting, and management of human-induced seismicity at Preston New Road, Lancashire, England. *Seismological Research Letters*, 90(5), 1902–1915.
- Clerc, F., Harrington, R. M., Liu, Y., & Gu, Y. J. (2016). Stress drop estimates and hypocenter relocations of induced seismicity near Crooked Lake, Alberta. *Geophysical Research Letters*, 43, 6942–6951. <https://doi.org/10.1002/2016GL069800>
- Davies, R., Foulger, G., Bindley, A., & Styles, P. (2013). Induced seismicity and hydraulic fracturing for the recovery of hydrocarbons. *Marine and Petroleum Geology*, 45, 171–185. <https://doi.org/10.1016/j.marpetgeo.2013.03.016>
- Dinske, C., & Shapiro, S. A. (2013). Seismotectonic state of reservoirs inferred from magnitude distributions of fluid-induced seismicity. *Journal of Seismology*, 17(1), 13–25. <https://doi.org/10.1007/s10950-012-9292-9>
- Dokht, R. M., Smith, B., Kao, H., Visser, R., & Hutchinson, J. (2020). Reactivation of an intraplate fault by mine-blasting events: Implications to regional seismic hazard in western Canada. *Journal of Geophysical Research: Solid Earth*, 125, e2020JB019933. <https://doi.org/10.1029/2020JB019933>
- Eaton, D. W., & Schultz, R. (2018). Increased likelihood of induced seismicity in highly overpressured shale formations. *Geophysical Journal International*, 214(1), 751–757. <https://doi.org/10.1093/gji/ggy167>
- Efron, B. (1982). *The Jackknife, the bootstrap and other resampling plans*. Philadelphia, PA: Society for Industrial and Applied Mathematics.
- Ellsworth, W. L. (2013). Injection-induced earthquakes. *Science*, 341(6142), 1225942. <https://doi.org/10.1126/science.1225942>
- Ester, M., Kriegel, H.-P., Sander, J., & Xu, X. (1996). A density-based algorithm for discovering clusters in large spatial databases with noise. In *Knowledge discovery and data mining* (Vol. 96, pp. 226–231).
- Farahbod, A. M., Kao, H., Cassidy, J. F., & Walker, D. (2015). How did hydraulic-fracturing operations in the Horn River Basin change seismicity patterns in northeastern British Columbia, Canada? *The Leading Edge*, 34(6), 658–663. <https://doi.org/10.1190/tle34060658.1>
- Fereidoni, A., & Atkinson, G. M. (2017). Discriminating earthquakes from quarry blasts based on ShakeMap ground-motion parameters. *Bulletin of the Seismological Society of America*, 107(4), 1931–1939.
- Frias-Martinez, E., Chen, S. Y., & Liu, X. (2006). Survey of data mining approaches to user modeling for adaptive hypermedia. *IEEE Transactions on Systems, Man, and Cybernetics, Part C*, 36(6), 734–749. <https://doi.org/10.1109/tsmc.2006.879391>
- Galloway, E., Hauck, T., Corlett, H., Panä, D., & Schultz, R. (2018). Faults and associated karst collapse suggest conduits for fluid flow that influence hydraulic fracturing-induced seismicity. *Proceedings of the National Academy of Sciences of the United States of America*, 115(43), E10003–E10012. <https://doi.org/10.1073/pnas.1807549115>
- Goebel, T. H. W., Hauksson, E., Aminzadeh, F., & Ampuero, J.-P. (2015). An objective method for the assessment of fluid injection-induced seismicity and application to tectonically active regions in central California. *Journal of Geophysical Research: Solid Earth*, 120, 7013–7032. <https://doi.org/10.1002/2015JB011895>
- Goebel, T. H. W., Weingarten, M., Chen, X., Haffener, J., & Brodsky, E. E. (2017). The 2016 Mw 5.1 Fairview, Oklahoma earthquakes: Evidence for long-range poroelastic triggering at >40 km from fluid disposal wells. *Earth and Planetary Science Letters*, 472, 50–61. <https://doi.org/10.1016/j.epsl.2017.05.011>
- Gutenberg, B., & Richter, C. F. (1944). Frequency of earthquakes in California. *Bulletin of the Seismological Society of America*, 34(4), 185–188.
- Hajati, T., Langenbruch, C., & Shapiro, S. (2015). A statistical model for seismic hazard assessment of hydraulic-fracturing-induced seismicity. *Geophysical Research Letters*, 42, 10601–10606. <https://doi.org/10.1002/2015GL066652>
- Hallo, M., Opsal, I., Eisner, L., & Ali, M. Y. (2014). Prediction of magnitude of the largest potentially induced seismic event. *Journal of Seismology*, 18(3), 421–431. <https://doi.org/10.1007/s10950-014-9417-4>

- Hashemzadeh, M., Golzari Oskouei, A., & Farajzadeh, N. (2019). New fuzzy C-means clustering method based on feature-weight and cluster-weight learning. *Applied Soft Computing*, 78, 324–345. <https://doi.org/10.1016/j.asoc.2019.02.038>
- Healy, J. H., Rubey, W. W., Griggs, D. T., & Raleigh, C. B. (1968). The Denver earthquakes. *Science*, 161(3848), 1301–1310. <https://doi.org/10.1126/science.161.3848.1301>
- Hincks, T., Aspinall, W., Cooke, R., & Gernon, T. (2018). Oklahoma's induced seismicity strongly linked to wastewater injection depth. *Science*, 359(6381), 1251–1255. <https://doi.org/10.1126/science.aap7911>
- Hsieh, P. A., & Bredehoeft, J. D. (1981). A reservoir analysis of the Denver earthquakes: A case of induced seismicity. *Journal of Geophysical Research*, 86(B2), 903–920. <https://doi.org/10.1029/JB086iB02p00903>
- Hubbard, S., Pemberton, S., & Howard, E. (1999). Regional geology and sedimentology of the basal Cretaceous Peace River Oil Sands deposit, north-central Alberta. *Bulletin of Canadian Petroleum Geology*, 47(3), 270–297.
- Kao, H., Eaton, D., Atkinson, G., Maxwell, S., & Mahani, A. B. (2016). Technical meeting on the Traffic Light Protocols (TLP) for induced seismicity: Summary and recommendations. *Geological Survey of Canada, Open File*, 8075, 20.
- Kao, H., Hyndman, R., Jiang, Y., Visser, R., Smith, B., Babaie Mahani, A., et al. (2018). Induced seismicity in western Canada linked to tectonic strain rate: Implications for regional seismic hazard. *Geophysical Research Letters*, 45, 11104–11115. <https://doi.org/10.1029/2018GL079288>
- Kao, H., Visser, R., Smith, B., & Venables, S. (2018). Performance assessment of the induced seismicity traffic light protocol for northeastern British Columbia and western Alberta. *The Leading Edge*, 37(2), 117–126. <https://doi.org/10.1190/tle37020117.1>
- Keranen, K. M., Weingarten, M., Abbers, G. A., Bekins, B. A., & Ge, S. (2014). Sharp increase in central Oklahoma seismicity since 2008 induced by massive wastewater injection. *Science*, 345(6195), 448–451. <https://doi.org/10.1126/science.1255802>
- Langenbruch, C., & Zoback, M. D. (2016). How will induced seismicity in Oklahoma respond to decreased saltwater injection rates? *Science Advances*, 2(11), e1601542. <https://doi.org/10.1126/sciadv.1601542>
- Lomax, A., Virieux, J., Volant, P., & Berge-Thierry, C. (2000). Probabilistic earthquake location in 3D and layered models. In *Advances in seismic event location* (pp. 101–134). Berlin, Heidelberg: Springer.
- Martínez-Garzón, P., Kwiatek, G., Sone, H., Bohnhoff, M., Dresen, G., & Hartline, C. (2014). Spatiotemporal changes, faulting regimes, and source parameters of induced seismicity: A case study from the Geysers geothermal field. *Journal of Geophysical Research: Solid Earth*, 119, 8378–8396. <https://doi.org/10.1002/2014JB011385>
- Maxwell, S., Jones, M., Parker, R., Miiong, S., Leaney, S., Dorval, D., et al. (2009). Fault activation during hydraulic fracturing. In *SEG Technical Program Expanded Abstracts 2009* (pp. 1552–1556). Society of Exploration Geophysicists.
- Norbeck, J. H., & Rubinstein, J. L. (2018). Hydromechanical earthquake nucleation model forecasts onset, peak, and falling rates of induced seismicity in Oklahoma and Kansas. *Geophysical Research Letters*, 45, 2963–2975. <https://doi.org/10.1002/2017GL076562>
- Pawley, S., Schultz, R., Playter, T., Corlett, H., Shipman, T., Lyster, S., & Hauck, T. (2018). The geological susceptibility of induced earthquakes in the Duvernay Play. *Geophysical Research Letters*, 45, 1786–1793. <https://doi.org/10.1002/2017GL076100>
- Pei, S., Peng, Z., & Chen, X. (2018). Locations of injection-induced earthquakes in Oklahoma controlled by crustal structures. *Journal of Geophysical Research: Solid Earth*, 123, 2332–2344. <https://doi.org/10.1002/2017JB014983>
- Peña Castro, A., Roth, M., Verdecchia, A., Onwuemeka, J., Liu, Y., Harrington, R., et al. (2020). Stress chatter via fluid flow and fault slip in a hydraulic fracturing-induced earthquake sequence in the Montney Formation, British Columbia. *Geophysical Research Letters*, 47, e2020GL087254. <https://doi.org/10.1029/2020GL087254>
- Roth, M. P., Verdecchia, A., Harrington, R. M., & Liu, Y. (2020). High-resolution imaging of hydraulic-fracturing-induced earthquake clusters in the Dawson-Septimus area, Northeast British Columbia, Canada. *Seismological Research Letters*, 91(5), 2744–2756. <https://doi.org/10.1785/02202000086>
- Rubinstein, J. L., & Mahani, A. B. (2015). Myths and facts on wastewater injection, hydraulic fracturing, enhanced oil recovery, and induced seismicity. *Seismological Research Letters*, 86(4), 1060–1067. <https://doi.org/10.1785/0220150067>
- Schorlemmer, D., Neri, G., Wiemer, S., & Mostaccio, A. (2003). Stability and significance tests for b-value anomalies: Example from the Tyrrhenian Sea. *Geophysical Research Letters*, 30(16), 1835. <https://doi.org/10.1029/2003GL017335>
- Schubert, E., Sander, J., Ester, M., Kriegel, H. P., & Xu, X. (2017). DBSCAN Revisited, Revisited. *ACM Transactions on Database Systems*, 42(3), 1–21. <https://doi.org/10.1145/3068335>
- Schultz, R., Atkinson, G., Eaton, D. W., Gu, Y. J., & Kao, H. (2018). Hydraulic fracturing volume is associated with induced earthquake productivity in the Duvernay Play. *Science*, 359(6373), 304–308. <https://doi.org/10.1126/science.aoa0159>
- Schultz, R., Corlett, H., Haug, K., Kocon, K., MacCormack, K., Stern, V., & Shipman, T. (2016). Linking fossil reefs with earthquakes: Geologic insight to where induced seismicity occurs in Alberta. *Geophysical Research Letters*, 43, 2534–2542. <https://doi.org/10.1002/2015GL067514>
- Schultz, R., Skoumal, R. J., Brudzinski, M. R., Eaton, D., Baptie, B., & Ellsworth, W. (2020). Hydraulic fracturing-induced seismicity. *Reviews of Geophysics*, 58, e2019RG000695. <https://doi.org/10.1029/2019RG000695>
- Schultz, R., Stern, V., & Gu, Y. J. (2014). An investigation of seismicity clustered near the Cordel Field, west central Alberta, and its relation to a nearby disposal well. *Journal of Geophysical Research: Solid Earth*, 119, 3410–3423. <https://doi.org/10.1002/2013JB010836>
- Schultz, R., Wang, R., Gu, Y. J., Haug, K., & Atkinson, G. (2017). A seismological overview of the induced earthquakes in the Duvernay Play near Fox Creek, Alberta. *Journal of Geophysical Research: Solid Earth*, 122, 492–505. <https://doi.org/10.1002/2016JB013570>
- Shapiro, S. A., & Dinske, C. (2009). Scaling of seismicity induced by nonlinear fluid-rock interaction. *Journal of Geophysical Research*, 114, B09307. <https://doi.org/10.1029/2008JB006145>
- Shapiro, S. A., Dinske, C., Langenbruch, C., & Wenzel, F. (2010). Seismogenic index and magnitude probability of earthquakes induced during reservoir fluid stimulations. *The Leading Edge*, 29(3), 304–309. <https://doi.org/10.1190/1.3353727>
- Shell Recovery Process. (2009). *Application for Approval of the Carmon Creek Project*. Volume 1: Project Description. Retrieved from <https://open.alberta.ca/publications/4458446>
- Stern, V., Schultz, R., Shen, L., Gu, Y., & Eaton, D. (2013). Alberta Earthquake Catalogue, Version 1.0: September 2006 through December 2010. *Alberta Geological Survey Open-File Rept*, 15, 36.
- Van der Baan, M., & Calixto, F. J. (2017). Human-induced seismicity and large-scale hydrocarbon production in the USA and Canada. *Geochemistry, Geophysics, Geosystems*, 18, 2467–2485. <https://doi.org/10.1002/2017GC006915>
- Van der Elst, N. J., Page, M. T., Weiser, D. A., Goebel, T. H. W., & Hosseini, S. M. (2016). Induced earthquake magnitudes are as large as (statistically) expected. *Journal of Geophysical Research: Solid Earth*, 121, 4575–4590. <https://doi.org/10.1002/2016JB012818>
- Verdon, J. P., & Budge, J. (2018). Examining the capability of statistical models to mitigate induced seismicity during hydraulic fracturing of shale gas reservoirs. *Bulletin of the Seismological Society of America*, 108(2), 690–701. <https://doi.org/10.1785/0120170207>

- Verdon, J. P., & Stork, A. L. (2016). Carbon capture and storage, geomechanics and induced seismic activity. *Journal of Rock Mechanics and Geotechnical Engineering*, 8(6), 928–935. <https://doi.org/10.1016/j.jrmge.2016.06.004>
- Visser, R., Kao, H., Smith, B., Goerzen, C., Kontou, B., Dokht, R., et al. (2020). A comprehensive earthquake catalogue for the Fort St. John-Dawson Creek region, British Columbia, 2017–2018. *Geological Survey of Canada, Open File*, 8718, 1. <https://doi.org/10.4095/326015>
- Visser, R., Smith, B., Kao, H., BabaieMahani, A., Hutchinson, J., & McKay, J. E. (2017). A comprehensive earthquake catalogue for northeastern British Columbia and western Alberta, 2014–2016. *Geological Survey of Canada, Open File*, 8335, 28. <https://doi.org/10.4095/306292>
- Wang, R., Gu, Y. J., Schultz, R., Zhang, M., & Kim, A. (2017). Source characteristics and geological implications of the January 2016 induced earthquake swarm near Crooked Lake, Alberta. *Geophysical Journal International*, 210(2), 979–988. <https://doi.org/10.1093/gji/ggx204>
- Weingarten, M., Ge, S., Godt, J. W., Bekins, B. A., & Rubinstein, J. L. (2015). High-rate injection is associated with the increase in U.S. mid-continent seismicity. *Science*, 348(6241), 1336–1340. <https://doi.org/10.1126/science.aab1345>
- Wiemer, S., & McNutt, S. R. (1997). Variations in the frequency-magnitude distribution with depth in two volcanic areas: Mount St. Helens, Washington, and Mt. Spurr, Alaska. *Geophysical Research Letters*, 24(2), 189–192. <https://doi.org/10.1029/96GL03779>
- Wiemer, S., & Wyss, M. (2000). Minimum magnitude of completeness in earthquake catalogs: Examples from Alaska, the western United States, and Japan. *Bulletin of the Seismological Society of America*, 90(4), 859–869. <https://doi.org/10.1785/0119990114>
- Yeck, W. L., Hayes, G. P., McNamara, D. E., Rubinstein, J. L., Barnhart, W. D., Earle, P. S., & Benz, H. M. (2017). Oklahoma experiences largest earthquake during ongoing regional wastewater injection hazard mitigation efforts. *Geophysical Research Letters*, 44, 711–717. <https://doi.org/10.1002/2016GL071685>
- Yu, H., Harrington, R. M., Liu, Y., & Wang, B. (2019). Induced seismicity driven by fluid diffusion revealed by a near-field hydraulic stimulation monitoring array in the Montney Basin, British Columbia. *Journal of Geophysical Research: Solid Earth*, 124, 4694–4709. <https://doi.org/10.1029/2018JB017039>